J Solid State Electrochem (2003) 7: 171–176
DOI 10.1007/s10008-002-0288-1

ORIGINAL PAPER

François Rouelle · Florence Toumelin-Chemla

Electrochemical corrosion kinetics of tin and tin amalgams in NaCl aqueous solutions

Received: 28 February 2002 / Accepted: 12 April 2002 / Published online: 6 June 2002

Abstract Electrochemical techniques were used to determine the corrosion rate of pure tin metal as compared to 80 Sn/20 Hg tin amalgam. X-ray diagrams showed that this amalgam was a crystalline γ_2 phase, whereas a 50 Sn/50 Hg amalgam contained liquid alloy embedded in the same γ_2 phase. Open circuit potential measurements, combined with narrow range potential scanning voltammetry, lead to the conclusion that amalgamation resulted in enhancement of the corrosion current, mainly by increasing the cathodic electron transfer reaction kinetics both in deaerated and in oxygen-saturated NaCl solution. When maintained at zero current potential in a solution containing dissolved O_2 gas, the samples were gradually covered with an insulating oxide layer which was identified by a series of electrochemical impedance diagrams recorded at different time intervals. The oxide layer was firmly adherent to the bulk tin metal but was poor at protecting the amalgam electrode. Finally, at potential values where the anodic current reached a few mA/cm^2, the pure tin metal surface was suddenly deteriorated by the formation of extremely deep pinhole corrosion pits, while this effect was smoothed down by amalgamation.

Keywords Electrochemical corrosion · Tin · Amalgams · Impedance

Introduction

The metallurgy of tin has been known from the earliest ages of mankind. This metal is very suitable in many important applications, owing to its main properties such as low melting point, malleability, good resistance to corrosion, and its non-toxic nature in the food processing industry and environmental regulations. It was postulated that the extremely low corrosion rate was due to the presence of a thin, stable passive film that forms on the metal surface [1]. For this reason, most of the electrochemical studies dealing with tin surface properties are devoted to the physical properties of these oxide layers. Indeed, tin oxides have been shown to behave as semiconductor materials. Depending on the pH of the solution and the potential for anodization, the stoichiometric composition of the oxide [2] could vary from $Sn(OH)_2$ and $SnO.xH_2O$ to $Sn(OH)_4$ and SnO_2. When prepared in a phosphate buffer electrolyte, the composition of the passive film studied by X-ray diffraction contained $Sn_3(PO_4)_2$ together with a mixture of SnO and SnO_2 oxides [3]. Several high-performance techniques, such as X-ray photoelectron spectroscopy, photoelectrochemistry [1, 4], photocurrent spectroscopy [5], and Fourier transform infrared spectroscopy, were used to characterize these oxides; they are generally described as amorphous, heavily doped n-type semiconductors whose growth involves a field-assisted migration of ions through the oxide [6].

However, although the corrosion kinetics of tin and tin-plated metals in organic acids, their salts and food systems containing these acids has been the subject of considerable work [7], very few prior studies dealing with the corrosion kinetics of tin in saline solution are available. Only qualitative data are given [8], indicating that local corrosion occurs in salt solutions which do not form insoluble compounds with stannous ions (e.g. chloride, bromide, sulfate), but is unlikely in solutions giving stable precipitates (borate, phosphate, carbonate). After a few days, this local dissolution will lead to pitting corrosion.

In the present study, we investigated the kinetics of tin corrosion near the open circuit potential (OCP) in NaCl solutions, either carefully deaerated or oxygen saturated, aiming at obtaining quantitative measurements

F. Rouelle (✉)
Laboratoire d'Electrochimie, LI2C Boite 51,
Université Pierre et Marie Curie, 4 Place Jussieu,
75252 Paris Cedex 05, France
E-mail: rouelle@cicrp.jussieu.fr

F. Toumelin-Chemla
Département des Biomatériaux,
Faculté d'Odontologie, Université Paris V,
1 Rue Maurice Arnoux, 92120 Montrouge, France

and new insights on the electrochemical reactions which take place at the metal/electrolyte interface. The main techniques used in this study were voltammetry and electrochemical impedance spectrometry (EIS), using a rotating disc electrode. Moreover, for the first time, the same investigation was extended to tin amalgam alloys; the results of this study could lead to a better understanding of dealloying processes which are recognized to occur during ageing of dental amalgams [9] in oral media. Dealloying of tin amalgams was clearly demonstrated by a remarkable technique of abrasive stripping voltammetry [10], showing two perfectly separated peaks of Sn and Hg oxidation in the Hg/Sn γ_2 phase. On the other hand, the influence of amalgamation on the electrochemical reactivity of pure metals, for example amalgamated zinc electrodes in alkaline batteries [11, 12, 13], could be derived from electron transfer kinetics.

Experimental

Three kinds of samples were used in this study:

1. Pure Sn metal.
2. Solid state Sn amalgam, 80/20 wt%, which corresponds very closely to the $Sn_{6-7}Hg$ γ_2 phase [14]. This special structure, different from pure Sn (Fig. 1a), was checked by X-ray diffraction as shown in Fig. 1b.
3. Solid state Sn amalgam, 50/50 wt%. The X-ray diagram shown in Fig. 1c contains the same lines as in Fig. 1b, surrounded by a wide background characteristic of an amorphous phase. The examination of the mechanic properties of this alloy seems to indicate the presence of microparticles of liquid tin amalgam embedded in the matrix of the γ_2 phase.

All the measurements were undertaken following a classical procedure. The metal samples were prepared by melting under vacuum, in a glass tube, and then cast in a mould to form a cylindrical piece 4 mm in diameter. These samples, pure Sn or solid state Sn/Hg alloys (80/20 and 50/50 wt%), were inserted in a Teflon tip, the surface being then polished before each experiment, to form a rotating disk electrode (Fig. 2). The surface was finished with a wet plastic film covered with 0.3 μm alumina particles. The rotating device was an EDI 101T driven by a controlled speed generator (CTV 101T, Radiometer Analytical). Most generally, the rotation speed was fixed to 3000 rpm, for which the usually adopted limiting diffusion layer is 10 μm thick. The experiments were carried at room temperature, which was checked to be quite stable at 21.0 ± 0.2 °C.

All chemicals, NaCl, Sn, and Hg, were of high purity, produced by Johnson-Matthey. The solutions were prepared with ultrapure deionized water (UPW) of 18.2 MΩ resistivity. Depending on the experimental conditions, the solution was deoxygenated beforehand by bubbling pure argon gas (N60 grade, L'Air Liquide), containing less than 0.1 ppm residual oxygen, for at least 1 h. Alternatively, in order to examine the influence of dissolved O_2 under repeatable conditions, another series of experiments was undertaken using NaCl solutions saturated (40 ppm) with pure oxygen gas (N55 grade) at atmospheric pressure. In these conditions the composition of the electrolyte was perfectly defined. The pH value of the solution was carefully checked and found equal to 5.90 ± 0.10.

The experiments were carried out in a glass electrochemical cell, using a platinum counter electrode and a saturated calomel reference electrode. The whole cell was roughly protected against room light, although preliminary experiments proved that there was a quite negligible effect of light despite the semiconducting properties of the oxide layer [5]. Electrochemical parameters obtained by linear voltammetry were determined with a Tacussel Radiometer Analytical PGS 201T potentiostat. This device was driven by an IBM PC computer using Voltamaster software, which includes several electrochemical programs such as zero current open circuit potential, chronoamperometry at constant voltage, polarization resistance, and cyclic voltammetry. For each run, numerical data were recorded in memory files in the same computer, and used

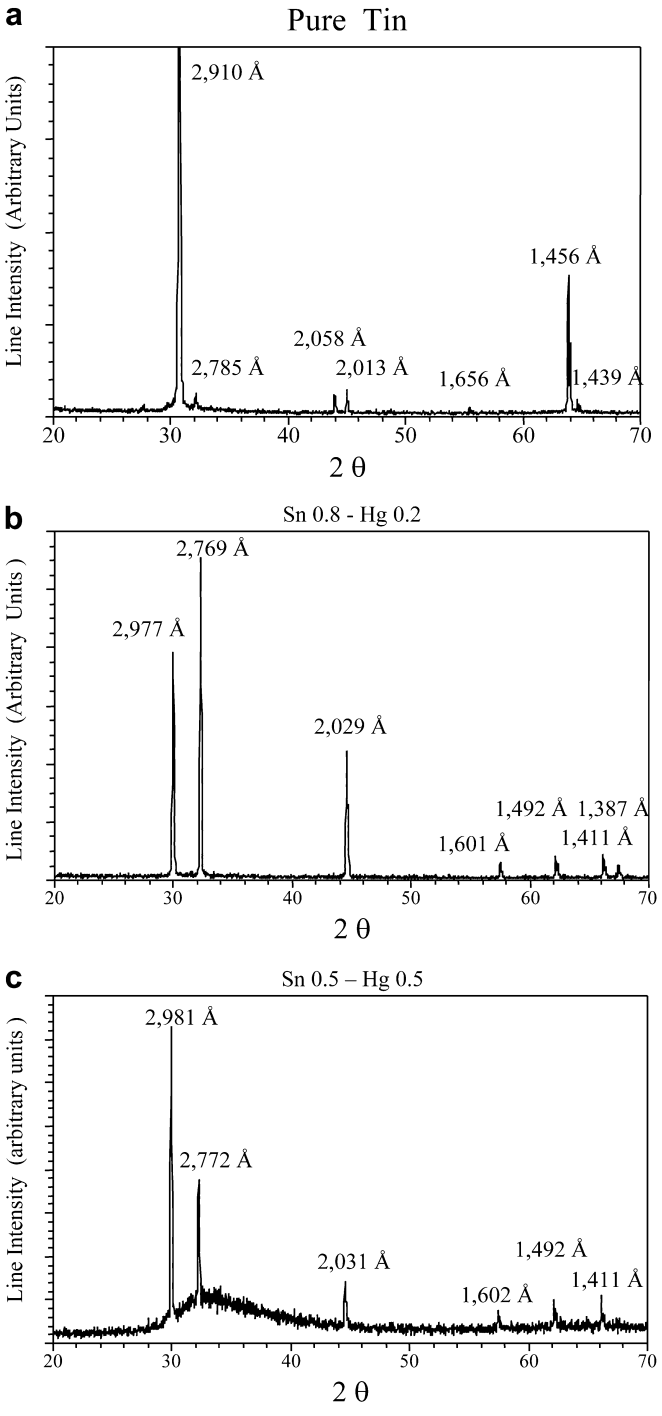

Fig. 1 **a** Tin metal X-ray diffraction diagram. **b** Sn 80/Hg 20 γ_2-phase amalgam diffraction diagram. **c** Sn 50/Hg 50 tin amalgam diffraction diagram

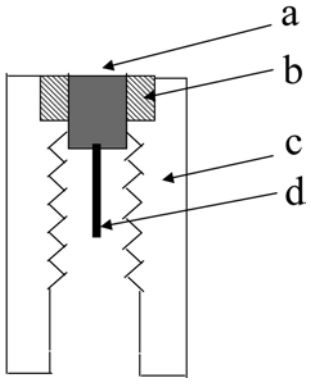

Fig. 2 Rotating disk electrode tip: *a*, metal sample; *b*, polymerized epoxide resin; *c*, Teflon tip; *d*, electrical contact to EDI 101T rotating device

either for drawing the corresponding graphs or for a mathematical simulation leading to an interpretation model.

The electrochemical impedance parameters were obtained using an EG&G PAR model 273A potentiostat connected to a vectorial impedance analyser (Solartron 1260). Depending on the interface properties, the frequency range was scanned from 10^5 to 10^{-3} Hz. However, in some experiments, in order to follow the impedance variation versus time, the frequency range was chosen so as to record a full impedance diagram within 2 min, typically from 40 to 10^{-2} Hz, a procedure which was checked beforehand to correspond to the main RC loop. Again, numerical data were recorded in a memory file within the driving IBM PC. The equivalent circuits were modelled by a series of resistance and constant phase element (CPE) loops whose values were obtained either by the software Zplot included in the impedance Solartron equipment or using the Boukamp [19] software recorded in a separate computer.

Results and discussion

Before each potential scanning experiment, the OCP of Sn and Hg/Sn alloys in the solution was recorded during 10–20 min to check the stability and reliability of the initial surface state of the metal sample. Measurements in both deaerated or oxygen saturated NaCl solutions were quite reproducible; the obtained values are presented in Table 1.

The experimental conditions, a narrow range of potentials around the OCP, are such that the anodic charge transfer reaction should be:

$$Sn + 2H_2O \rightleftarrows Sn(OH)_2 + 2H^+ + 2e^- \quad (1)$$

whose standard thermodynamic potential is [15]:

Table 1 Open circuit potentials of Sn and Sn amalgams; mV versus SCE

Sample	Deaerated solution	Oxygen-saturated solution
Pure Sn	–605 ± 5	–450 ± 10
Sn/Hg (80/20 wt%)	–540 ± 10	–460 ± 10
Sn/Hg (50/50 wt%)	–535 ± 20	–485 ± 20

$$E^\circ_{Sn/Sn(OH)_2} = -0.091 - 0.059\ \text{pH V/SHE} \quad (2)$$

i.e. $E^\circ_{Sn/Sn(OH)_2} = -0.680$ V/SCE at pH 5.9.

The deviation of the experimental values from the thermodynamic data concerning pure Sn is rather small and must be assigned to kinetic parameters involved in the corrosion process. This behaviour is characteristic of a mixed potential where the kinetics rate constant k_0 of the anodic reaction is much more rapid than that of the cathodic process. When Sn is amalgamated the potential is expected to be more positive, but the order of magnitude of the shift, from a thermodynamics prediction, should be $-RT/2F \ln x$, i.e. less than 10 mV, whereas experimental data indicate +60 mV. The effect is quite clear for experiments carried in oxygen-saturated solutions, where all values of the OCP are shifted towards positive values. Indeed, in this case, the extremely small exchange current due to electrochemical reaction (1) is compensated by the reduction reaction of dissolved oxygen:

$$\tfrac{1}{2}\,O_2 + H_2O + 2e^- \rightleftarrows 2OH^-\ E^\circ_{O_2/OH^-} = 1.23 - 0.059\ \text{pH V/SHE} \quad (3)$$

Then the OCP mixed potential E_r, derived from the steady regime of the anodic and cathodic corrosion currents, is given by the expression:

$$E_r = \frac{\alpha_A E^\circ_{Sn/Sn(OH)_2} + \alpha_C E^\circ_{O_2/OH^-}}{\alpha_A + \alpha_C} + \frac{RT}{(\alpha_A + \alpha_C)} \ln \frac{i^\circ_{O_2}}{i^\circ_{Sn}} \quad (4)$$

where α_A and α_C are the transfer coefficients for anodic and cathodic electron transfer, and i°_{Sn} and $i^\circ_{O_2}$ are the exchange current densities for the anodic and cathodic processes.

In other respects, a deep analysis of the parameters should include the possible variation of the local pH at the interface. However, in general, at OCP, i.e. zero current potential, the local lowering of the pH associated with the tin ionization (Eq. 1) is exactly compensated by the associated cathodic reaction, proton reduction in deaerated solution, or OH^- generation in oxygenated solution. Nevertheless, this effect must be taken into account in voltammetry, when a net anodic current is observed.

The interpretation based on the electrochemical reaction rates is well illustrated by a study of the voltammograms in a rather large potential range in order to obtain the linear variation of the current density in the log scale and to derive the values of i° corresponding to anodic and cathodic site electron transfer. Figure 3 shows the Tafel diagrams obtained in a deaerated NaCl solution for pure tin metal and for the γ_2 phase amalgam, respectively. Results with 50/50 amalgam are not presented because we obtained scattered graphs which were attributed to the inhomogeneous structure of this alloy. From the diagrams of Fig. 3, the Tafel slope of the cathodic branch on both samples indicates that the

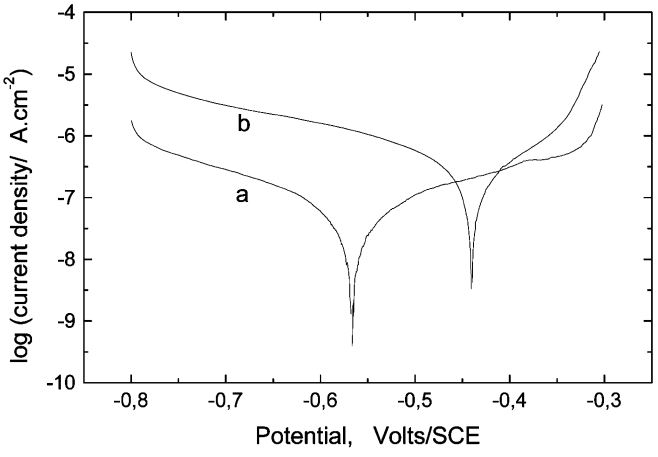

Fig. 3 Tafel diagrams for voltammetry in deaerated NaCl solution: *a* pure tin metal; *b* γ_2 phase tin amalgam

charge transfer reaction is controlled by an activation step. Moreover, it is readily demonstrated that the cathodic current intensity on the amalgam is much higher than on the pure metal. This conclusion is inconsistent with the general assumption that metal amalgamation should inhibit the cathodic hydrogen evolution reaction [12].

In a second step, the corrosion current density was evaluated from a series of polarization resistances derived from the slope of the graphs obtained by a narrow voltammetry range near the zero current potential. In this case the samples were polished to produce a new fresh surface just before the measurement.

Comparison of the experimental data obtained with pure Sn and Sn amalgams led to a surprising new result, as indicated in Table 2. In fact, from these data it is clearly shown that the polarization resistance, $R_p(\partial E/\partial i)_{i=0}$, decreases in the order pure Sn, 80/20 Sn amalgam, 50/50 Sn amalgam. The values of the corrosion current, i_{corr}, derived from the relation:

$$i_{corr} = i_{Sn} = i^{\circ}_{Sn} \exp\left(\frac{\alpha_A F\left(E_r - E^{\circ}_{Sn/Sn(OH)_2}\right)}{RT}\right) = \frac{RT}{(\alpha_A + \alpha_C)FR_p} \quad (5)$$

are listed in Table 2.

In a series of preliminary experiments it was readily recognized that the results for both the OCP and the corrosion current density were dependent on the disc electrode rotation, although we could expect that the formation of an insoluble oxide layer should be independent of the hydrodynamic conditions. In fact the main effect was linked to the adhesion of this oxide on the metal substrate surface, and this is now developed hereafter.

Table 2 Corrosion current density of Sn and Sn/Hg alloys in NaCl solutions

Sample	Deaerated solution (A/cm^2)	Oxygen-saturated solution (A/cm^2)
Pure Sn	1.04×10^{-7}	2.28×10^{-7}
Sn/Hg (80/20 wt%)	4.64×10^{-7}	6.16×10^{-7}
Sn/Hg (50/50 wt%)	9.1×10^{-7}	11.9×10^{-7}

The electrochemical response of pure tin metal in voltammetry shows the reversibility of the redox reaction leading to stannous oxide, provided the scanning of potential is carried on under strictly defined conditions:

1. The potential scanning must be not too slow in order to hinder a gradual growth of the insulating layer which contributes to smoothen the oxidation peak. In Fig. 4 the scan rate was 1 V/min.
2. Another important parameter is that the anodic limit of the scan must be strictly defined. Even a few millivolts more positive value leads to pitting corrosion following the mechanism of local acidification [16]:

$$Sn \rightarrow Sn^{2+} + 2e^- \quad (6)$$

$$Sn^{2+} + 4H_2O \rightleftarrows Sn(OH)_2 + 2H_3O^+ \quad K_s = 3\times10^{-27} \quad (7)$$

The generated pH gradient can be estimated from the relation:

$$i = 2FD_{H_3O^+}\mathrm{grad}C_{H_3O^+} \quad (8)$$

Owing to the extremely low solubility product of $Sn(OH)_2$, the local pH at the metal interface can reach values as low as pH 2, a solution in which Sn^{2+} ions are readily soluble. In the case of pure Sn metal, we observed the appearance of extremely thin and deep pinhole pits only visible with a metallographic microscope. In this situation, the graph shown in Figs. 3 and 4 cannot be reproduced.

The growth of the protecting oxide layer was subsequently studied by a series of potential scans in a

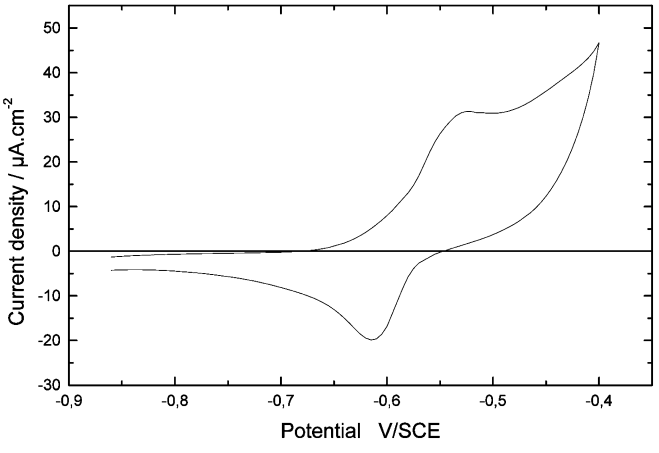

Fig. 4 Cyclic voltammetry of Sn in deaerated NaCl solution; scan rate 1 V/min

narrow range of ±30 mV around the OCP during 24 h. The experiment was carried on in the same NaCl solution saturated with O_2 gas, which contributed to stabilize the SnO by transformation into SnO_2. The remarkable results obtained in this experiment are summarized in Fig. 5, showing clearly a gradual shift of the OCP towards more positive values, with a simultaneous decrease of the slope $\Delta i/\Delta E$, thus characterizing a corresponding increase of the oxide resistivity.

A more precise evaluation of this oxide growth was obtained by EIS in a series of diagrams recorded at the OCP. Figure 6 shows the variation of Nyquist impedance diagrams obtained with pure tin metal, in an O_2-saturated NaCl solution, as a function of time at intervals of about 1 h each. The main general feature is that we observe a net increase of the overall impedance versus time. Such a series of semi-circular diagrams is typical of a growing surface oxide protecting layer [17]. For a better analysis of the contributions of the involved components, we used a rather simplified model generally

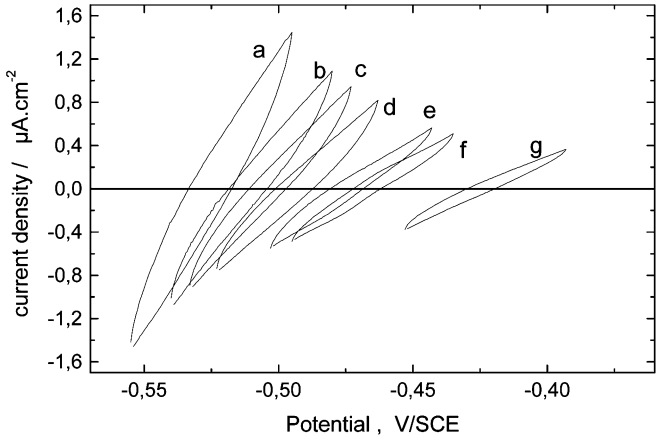

Fig. 5 Successive narrow range (60 mV) potential scans for Sn in oxygen-saturated NaCl solution: *a*, first scan; *b–g*, subsequent scans at about 1 h intervals

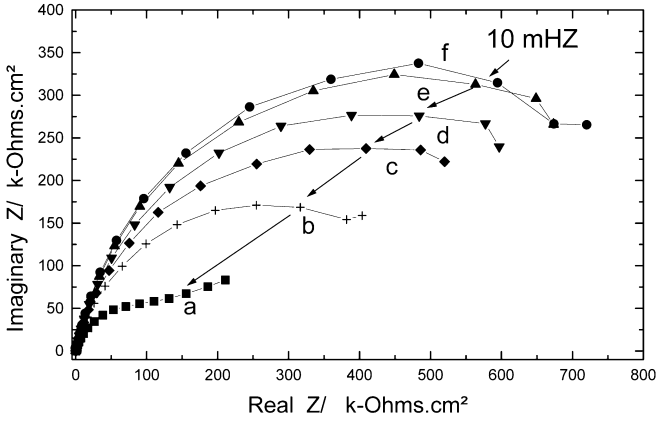

Fig. 6 Successive Nyquist impedance diagrams for pure Sn in oxygen-saturated NaCl solution: *a*, first diagram; *b–f*, subsequent diagrams at about 1 h intervals

considered as well adapted to corrosion processes [18], such as is given in Fig. 7. The overall impedance can be written [18]:

$$Z(\omega) = R_s + 1/[j\omega C_d(\omega) + 1/(R_T + Z_W(\omega))] \quad (9)$$

In this expression, R_s represents the series resistance due mainly to the electrolyte solution, $C_d(\omega)$ is the double layer capacitance, which is generally observed, in corroding systems, as being a CPE whose impedance is expressed as:

$$Z_{CPE} = Q(j\omega)^{-n} \quad (10)$$

where Q is equivalent to the reciprocal of a capacitance, and n a parameter indicating the deviation from a perfect capacitor ($n = 1$ represents a pure capacitance). Generally, $n \leq 1$ was considered as reflecting the roughness of the electrode surface. More recently [18] the effect was assigned to a frequency dependence obeying a Debye-type dispersion. In this classical model, R_T designates the transfer resistance and Z_W the Warburg impedance including the transport of electroactive species.

In the frame of this model, the results of Fig. 6 showing a gradual increase of the overall impedance can be interpreted as follows. As a rather insulating oxide layer is thickening, the double layer capacitance is modified by a series capacitor formed by the metal/oxide/electrolyte (MOE) junction. Then the observed capacitance decreases with time. On the other hand, the term R_T is increased by the resistive properties of this oxide as a result of the hindered transport of electroactive species. This oxide layer growth is faster in oxygen-saturated solutions and contributes to limit the increase of the corrosion rate in this solution. Finally, the Z_W term is only visible at low frequency values, just at the beginning of the experiment (curve a) when the R_T value is small enough. As R_T increases with time, the term Z_W tends to be negligible. This interpretation was checked by the quantitative determination of the main components of the equivalent circuit, using the Boukamp [19] software. The adjusted parameters (Table 3) fitted the experimental data with a significance test $\chi^2 \approx 10^{-3}$, the term R_s being almost constant as predicted by the model.

Figure 8 shows that similar results were also obtained with a non-rotating (80 Sn/20 Hg) tin amalgam electrode, but the impedance values were half that obtained with pure tin metal. Moreover, we observed that the

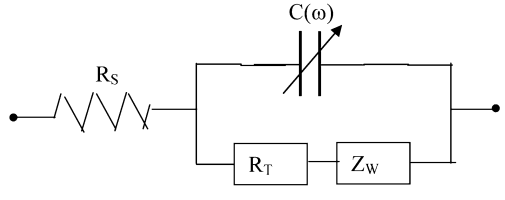

Fig. 7 Equivalent circuit used to model the corroding metal/solution interface

Table 3 Values of the impedance components of the equivalent circuit (Fig. 6)

Time (h)	R_s (Ω)	R_T (kΩ)	$1/Q$ (μF)	N
~0.5	92.1	153	13.5	0.81
4	91.6	631	9.1	0.83
10	89.4	913	6.55	0.84

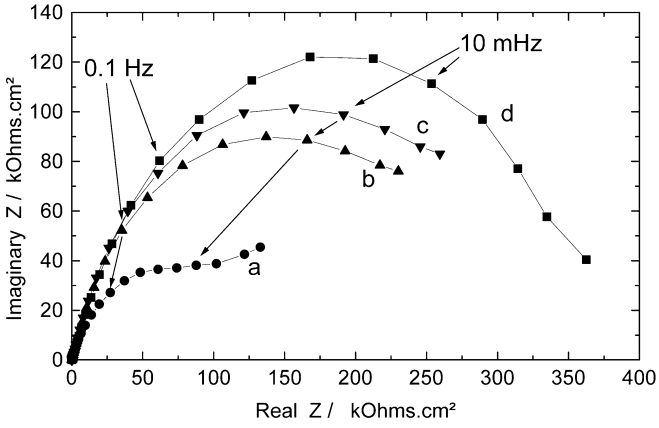

Fig. 8 Successive Nyquist impedance diagrams for γ_2 tin amalgam. Conditions similar to those of Fig. 6

oxide layer was much less adherent to the amalgam substrate than to the pure metal; indeed, the oxide protecting layer was easily detached from the amalgam by rotating the disc electrode at 3000 rpm. In other words, the lesser electrochemical reactivity of the bulk pure Sn metal than in the amalgam could be assigned to the more adherent and compact oxide layer on the pure solid tin metal.

Conclusion

This study of the corrosion rate of tin metal and the comparison with the solid state γ_2-phase tin amalgam lead to a better understanding of the change of electrochemical properties induced by metal amalgamation. One first result was the observed shift of the OCP towards more positive values following an increased rate constant of the cathodic electron transfer on the amalgam surface, a quite unexpected result since Hg metal is postulated to inhibit electrochemical reactions. Moreover the Sn oxidation current was not decreased by the concentration reduction induced by the amalgam dealloying process. The effect is related to the generation of a surface thin layer of liquid mercury nearly 0.1 μm thick. Then, knowing the diffusion coefficient [20] of Sn equal to 1.68 $cm^2\ s^{-1}$ in mercury, the limiting diffusion oxidation current could reach a value as high as 0.1 A cm^{-2}, a value higher than the experimental current density (generally a few μA cm^{-2}) by several orders of magnitude. A similar behaviour, almost equal to the rate constant, was observed in the comparison of the electrochemical properties of Zn metal and Zn amalgam [21]. As a consequence, we can easily understand that the intensity of the corrosion current is much higher for tin amalgam than for the bulk pure metal. On the other hand, the build-up of a compact oxide layer, identified by the gradual growth of the surface impedance, will contribute to protect the metal substrate and amplify the difference in the corrosion rate between the amalgam and the pure metal. These factors are quite consistent with the well-documented resistance to corrosion of tin metal. However, when the tin electrode potential is such that the anodic current density reaches values near 1 mA cm^{-2}, a pH gradient is set up at the interface and leads to the initiation of pits. The acid properties being maximum at the bottom of the pits, we observed the appearance of narrow extremely deep pinholes which result in a sudden rise of the corrosion process. In the case of amalgamated metal, this deleterious effect was significantly smoothed out by the transient generation of an extremely thin mercury layer.

Acknowledgements The authors are grateful to Prof. Ariel De Kozak and Ing. Jean-Paul Souron, Département de Cristallochimie du Solide, Université P. and M. Curie, for tin and tin amalgam X-ray diffraction patterns recorded on a vertical Philips PW 1050/25 goniometer mounted in the Bragg-Brentano configuration, with Ni filtered Cu Kα radiation.

References

1. Kapusta S, Hackerman N (1980) Electrochim Acta 25:1625
2. Seruga M, Melikos-Hukovic M, Valla T, Milun M, Hoffschultz H, Wandelt K (1996) J Electroanal Chem 407:83
3. Stirrup BN, Hampson NA (1976) J Electroanal Chem 73:189
4. Burleigh TD, Gerischer H (1988) J Electrochem Soc 135:2938
5. Moina CA, Varela FE, Feria Hernandez L, Ybarra GO, Vilche JR (1997) J Electroanal Chem 427:189
6. Metikos-Hukovic M, Omanovic S, Jukic A (1999) Electrochim Acta 45:977
7. Seruga M, Metikos-Hukovic M (1992) J Electroanal Chem 334:223
8. Hoar TP (1934) Trans Faraday Soc 30:472
9. Cohen F, Fiaud C, Chemla M (1988) C R Acad Sci Paris 307:733
10. Scholz F, Rabi F, Müller WD (1992) Electroanalysis 4:1992
11. Brodd RJ, Leger VE (1976) In: Bard AJ (ed) Encyclopedia of electrochemistry of the elements, vol 5. Dekker, New York, p 52
12. Jasinsky R (1967) High energy batteries. Plenum Press, New York, p 165
13. Zhang C, Wang JM, Zhang L, Cao CN (2001) J Electrochem Soc 148:E310
14. Eley BM (1997) Br Dent J 182:1997
15. Pourbaix M (1963) Atlas d'equilibres electrochimiques. Gauthier-Villars, Paris, p 477
16. Latimer WL (1952) Oxidation potentials. Prentice Hall, New York, p 148
17. Bertagna V, Erre R, Rouelle F, Levy D, Petitdidier S, Chemla M (2001) J Solid State Electrochem 5:306
18. Antano-Lopez R, Keddam M, Takenouti H (2001) Electrochim Acta 46:3611
19. Boukamp BA (1993) Equivalent circuit, version 4.51. University of Twente, The Netherlands
20. Cooper WC, Furman NH (1952) J Am Chem Soc 74:6183
21. Koryta J (1962) Electrochim Acta 6:62